Geochemistry Geophysics Geosystems G3
AN ELECTRONIC JOURNAL OF THE EARTH SCIENCES
Published by AGU and the Geochemical Society

Research Letter
Volume 8, Number 6
2 June 2007
Q06002, doi:10.1029/2006GC001437
ISSN: 1525-2027

Movement along a low-angle normal fault: The S reflector west of Spain

T. J. Reston
IFM-GEOMAR, Leibniz-Institute of Marine Sciences, Wischhofstrasse 1-3, D-20148 Kiel, Germany

Now at School of Geography, Earth and Environmental Sciences, University of Birmingham, B15 2TT Birmingham, UK (t.j.reston@bham.ac.uk)

T. Leythaeuser
IFM-GEOMAR, Leibniz-Institute of Marine Sciences, Wischhofstrasse 1-3, D-20148 Kiel, Germany

G. Booth-Rea
Departamento de Geodináamica, Universidad de Granada, Avenida Fuentenueva s/n, E-18071,Granada, Spain

D. Sawyer
Department of Earth Science, Rice University, MS-126, 6100 Main Street, Houston, Texas 77005, USA

D. Klaeschen and C. Long
IFM-GEOMAR, Leibniz-Institute of Marine Sciences, Wischhofstrasse 1-3, D-20148 Kiel, Germany

[1] The existence of normal faults that moved at low angles (less than 20°) has long been debated. One possible low-angle fault is the S detachment at the west Galicia (Spain) margin and thought to occur at the top of serpentinized mantle. It is unlikely that S was a large submarine slide as it was probably active over several million years without the development of any compressional features such as toe thrusts, it appears to have rooted beneath the conjugate Flemish Cap margin, and it is similar to structures elsewhere that also appear to be rooted detachments. Here we analyze depth images to identify synrift sediment packages above S and use the geometry of these synrift packages to constrain the angle at which S both formed and remained active. We find that S must have remained active at angles below 15°, too low to be explained simply by the low friction coefficient of partially serpentinized peridotites. Instead, we suggest that transient high fluid pressures must have developed within the serpentinites and propose a model in which anastomosing fault strands are alternately active and sealed, enabling moderately high fluid pressures to develop.

Components: 7425 words, 9 figures, 1 table.

Keywords: detachment faulting.

Index Terms: 8105 Tectonophysics: Continental margins: divergent (1212, 8124); 8118 Tectonophysics: Dynamics and mechanics of faulting (8004); 3025 Marine Geology and Geophysics: Marine seismics (0935, 7294).

Received 2 August 2006; **Revised** 29 January 2007; **Accepted** 15 March 2007; **Published** 2 June 2007.

Reston, T. J., T. Leythaeuser, G. Booth-Rea, D. Sawyer, D. Klaeschen, and C. Long (2007), Movement along a low-angle normal fault: The S reflector west of Spain, *Geochem. Geophys. Geosyst.*, *8*, Q06002, doi:10.1029/2006GC001437.

1. Introduction

[2] Low-angle normal (detachment) faults [*Wernicke*, 1981; *Westaway*, 1999] offer a means of efficiently extending the upper lithosphere tens of km along individual long-lived structures [*Forsyth*, 1992], but their existence and mechanics have been debated extensively in the literature. Some "low-angle" normal faults have been shown to be steeper structures passively rotated to low angle [*Buck and Lavier*, 2001; *Wernicke and Axen*, 1988]; others are associated with unusual tectonic conditions not widely applicable [*Westaway*, 1999]. Seismically active normal faults dipping at 30 ± 5° [*Abers*, 2001; *Rietbrock et al.*, 1996] such as the Moresby Detachment [*Mutter et al.*, 1996; *Floyd et al.*, 2001] do not address the issue, as such dips can be easily explained by the presence of moderately weak fault gouge [*Abers*, 2001]. The problem is thus twofold: whether normal faults active at less than ~25° exist [*Anders and Christie-Blick*, 1994] except in unusual tectonic settings [*Westaway*, 1999], and if so what are the mechanics of low-angle slip [e.g., *Axen*, 1992; *Wills and Buck*, 1997; *Westaway*, 1999].

[3] The S reflector west of the Galicia Bank (Figure 1) is the best known [*de Charpal et al.*, 1978; *Boillot et al.*, 1989; *Reston et al.*, 1996] of several possible low-angle faults [*Krawczyk et al.*, 1996; *Reston et al.*, 2004] occurring at the top of serpentinized mantle [*Zelt et al.*, 2003; *Whitmarsh et al.*, 2001; *Manatschal et al.*, 2001] at rifted margins. However, S and other similar structures have also been interpreted as ductile shear zones [*de Charpal et al.*, 1978; *Nagel and Buck*, 2004], as the crust-mantle boundary (CMB) offset by later steep faults [*Boillot et al.*, 1989], as the sole of large submarine landslides displacing crustal blocks over mantle exhumed at the seafloor [*Sawyer et al.*, 2005] and as steep normal faults rotated to low angles as part of a rolling hinge system [*Buck and Lavier*, 2001]. Here we use high quality data to show that the S reflector west of Spain [*de Charpal et al.*, 1978; *Reston et al.*, 1996] is a rooted, low-angle, normal fault that developed during continental breakup, and we propose a mechanism enabling low-angle slip. We use a combination of depth imaging, waveform inversion and numerical modeling to show that S was a brittle fault occurring at the contact between serpentinized mantle and overlying crustal fault blocks. The recognition of sedimentary wedges deposited during movement along S allows us to demonstrate that S was active at angles below 20°. Mechanically, this can be explained by the development of overpressure within fault strands sealed by the formation of serpentine in a crack/seal cycle. Our results may be applicable to other rifted margins and basins where similar structures have been observed [*de Charpal et al.*, 1978; *Krawczyk et al.*, 1996; *Reston et al.*, 2004] but not analyzed.

2. West Galicia Margin and the S Detachment

[4] The west Galicia margin formed by rifting and final separation between west Iberia and Flemish Cap during the early Cretaceous. The onset of rifting is thought to have occurred near the end of the Tithonian when rapid subsidence occurred and to have continued through several phases of faulting [*Reston*, 2005] into the Aptian: no clear spreading anomalies are observed west of the margin, consistent with the earliest seafloor being formed during the Cretaceous quiet zone.

[5] Seismic data show a series of tilted fault blocks above the bright S reflection. Previously published data [*de Charpal et al.*, 1978; *Boillot et al.*, 1989; *Reston et al.*, 1996] were collected with a weak source, and a 48 channel, 2.4 km streamer. The new data (Figures 2 and 3) were collected with a 4 km long, 160 channel streamer and a large airgun array, but even with better data, the imaging methods applied are crucial. The undulation and discontinuity of S on time migrations (Figure 2a) are distortions and imaging problems (velocity pull-up effects, focusing and defocusing) due to the passage of the seismic energy through the fault blocks and associated strongly laterally varying velocity structure. The solution is iterative prestack depth migration [*Reston et al.*, 1996] incorporating raypath bending not included in time migrations, and producing both a detailed velocity model above bright reflections such as S (Figures 2 and 3) and an undistorted depth image (Figures 2–4). The continuity of S is greatly improved and S appears as a sharp subhorizontal to slightly domal structure cutting to depth from a breakaway to the east. S passes underneath the high velocity fault blocks and intervening lower velocity half-grabens without being offset by the block-bounding faults that instead appear to detach onto S. Thus we interpret S as some form of detachment. The block-bounding faults themselves are imaged between adjacent

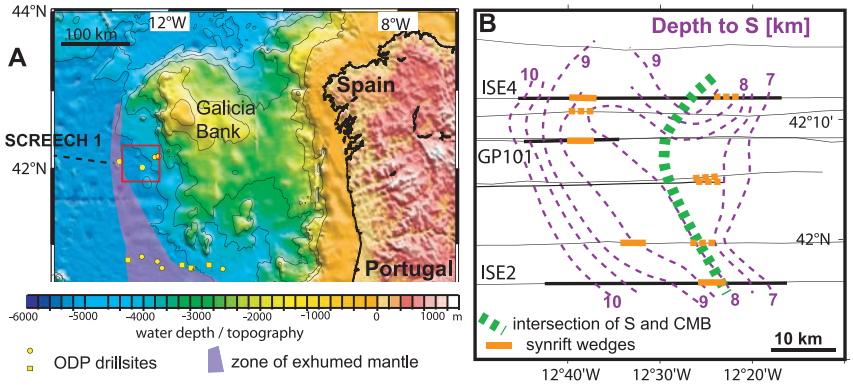

Figure 1. Location and form of the S detachment (red box) west of Iberia. (a) S occurs just to the east of a zone of exhumed continental mantle now largely covered with postrift sediment. Dashed line shows approximate relative location of the SCREECH 1 profile, shot on the conjugate Flemish Cap margin [*Hopper et al.*, 2004]. (b) Previous [*Reston et al.*, 1996] and new depth migrations of margin-normal profiles (black lines) allow the S reflector to be mapped out in three dimensions. Note that the dip direction of S deviates at most 45° from the profile direction for the data portions (bold) discussed here. Location of well-defined synrift sediment wedges marked in orange; note how these strike normal to the profiles.

blocks and can be traced up as exhumed slip surfaces at the western edge of successive fault blocks, onlapped by postrift sediments.

[6] Numerical modeling [*Pérez-Gussinyé and Reston*, 2001] shows that the entire extending crust becomes brittle when thinned to ~7 km (Figure 5). As S was active within 3 km of the seafloor, it cannot be a "ductile" shear zone deforming by creep. Further evidence that S is a brittle structure of some form comes from full waveform inversion [*Leythaeuser et al.*, 2005] (Figure 3), which shows that the S reflection is particularly sharp and of high amplitude (Figures 2 and 3) and that any apparent layering is due to residual airgun bubble reverberation. The reflector itself is characterized by a narrow (~50 m thick) low-velocity zone (LVZ) overlying a major step increase in seismic velocity corresponding to a major change in physical properties. However, S cannot be an evaporite (not reported from this margin) or shale decollement as it occurs within the basement. The overlying fault blocks have been sampled by drilling and by submersible, with granodiorite being recovered beneath a thin, tilted sequence directly above S. Wide-angle data [*Zelt et al.*, 2003] and PSDM consistently show that the core of the fault blocks have velocities between 5 and 6 km/s, too high for sedimentary rocks, but consistent with crystalline basement. Given its setting within basement at a hyperextended rifted margin, the velocities underlying S [*Zelt et al.*, 2003] and the outcrop of serpentinized peridotites just to the west, S is probably the boundary between crustal basement and underlying partially serpentinized mantle. Beneath S, the velocity derived from wide-angle data [*Zelt et al.*, 2003] increases gradually from below 7 km/s (~30% serpentinization) at ~9 km to 8 km/s (unserpentinized mantle) at ~12 km. This degree and thickness of serpentinization requires the uptake of ~200 m of water, which implies that over the minimum lateral extent of the S reflector (~1200 km^2; Figure 1), more than 150 km^3 of water may have been absorbed by the mantle. Such volumes can only be sourced from the surface, passing through the brittle crust along active faults

Figure 2. Seismic images and interpretation of the S reflector west of Spain. (a) Time migrated section of ISE4, showing distorted images of sedimentary geometries and of S. (b) Depth image of same data produced by PSDM, with detailed velocity structure overlain (see Figure 3 for velocity scale). Note how the distortions of the time image have been removed and how both the image and the velocity structure clearly define the S detachment, the overlying fault blocks, and the intervening wedges of sediment. (c) Interpretation of the depth section, with clearest synfaulting wedges colored orange. (d) Detail of fault (red dashed) detaching onto S (bold red dashed) and of sedimentary wedges developed above the active S detachment. These can be interpreted in terms of movement of the underlying block over (e) a flat-ramp-flat system where a steeper fault detaches onto the low-angle S. Although only the bright orange wedge is definitely fanning, the underlying pale orange and overlying yellow wedge may also have been deposited during movement along S. (f and g) The angles used to infer the geometry at which S was active (see Table 1).

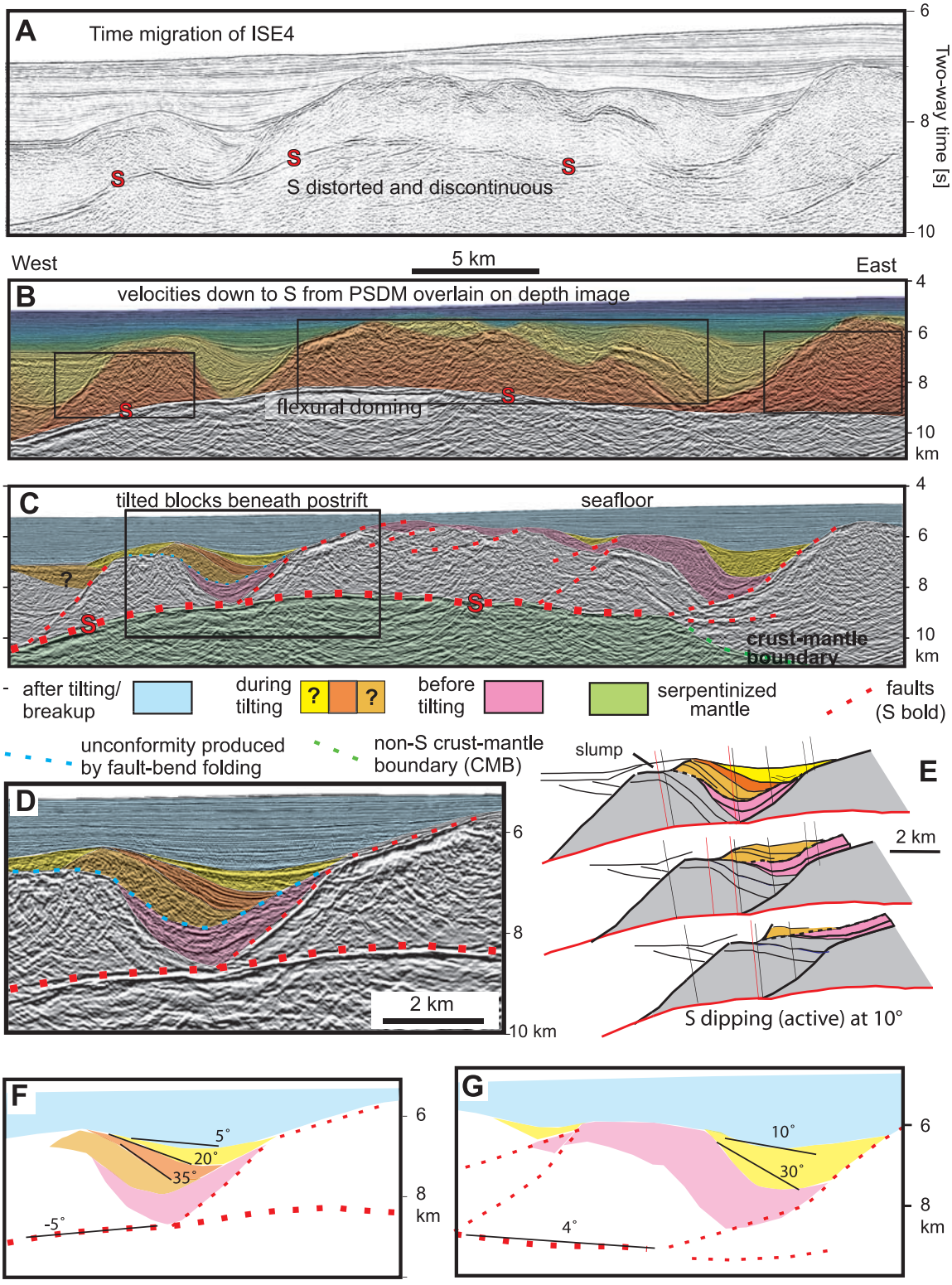
A
Time migration of ISE4
S
S
S
S distorted and discontinuous
6
8
10
Two-way time [s]
West
5 km
East
B
velocities down to S from PSDM overlain on depth image
S
flexural doming
S
4
6
8
10
km
C
tilted blocks beneath postrift
seafloor
?
S
S
crust-mantle boundary
4
6
8
10
km
after tilting/ breakup
during tilting
?
?
before tilting
serpentinized mantle
faults (S bold)
unconformity produced by fault-bend folding
non-S crust-mantle boundary (CMB)
D
6
8
2 km
10 km
slump
E
2 km
S dipping (active) at 10°
F
5°
20°
35°
-5°
6
8
km
G
10°
30°
4°
6
8
km

Figure 2

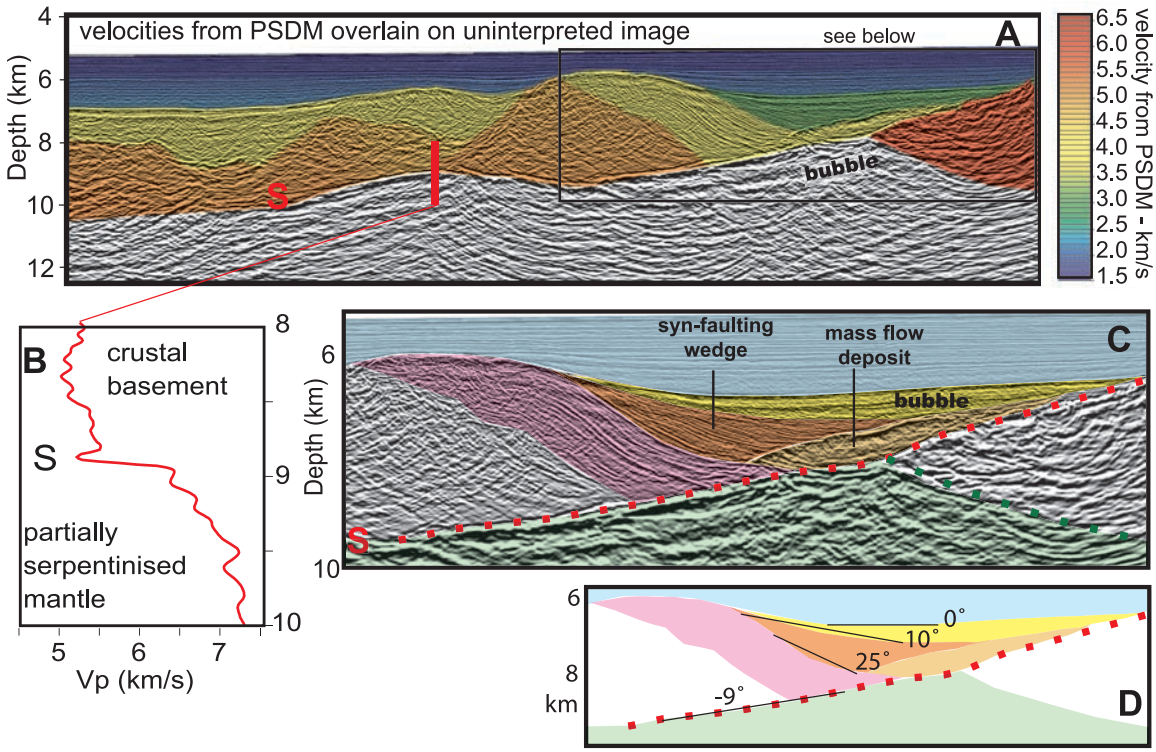

Figure 3. Depth image and velocity structure around S showing that it is a low-angle normal fault and a low-velocity zone. (a) Depth image at no vertical exaggeration produced by PSDM of profile ISE2 with detailed velocity structure down to S reflector overlain. Note how velocity structure defines the basement-cored (V > 5 km/s) fault blocks and the wedges of sediment infilling the half-grabens between blocks. (b) Detailed velocity structure across S produced by waveform inversion at location marked by red bar, showing that S is marked by a low-velocity zone (LVZ) above a major step increase in velocity [*Leythaeuser et al.*, 2005]. This is consistent with high fluid pressures during faulting. (c) Detail of sedimentary wedges abutting a lens of probable debris-flow deposits (paler orange) on the then-active S detachment (red dashed line). For key, see Figure 2. The orange section shows clear fanning toward the fault, implying that these units were deposited during movement along the fault. From the geometry it appears that S was active at <22.5°. The overlying yellow wedge may also be "synfaulting," but its internal structure is less clear due to residual bubble noise from the airgun source. If this is synrift, S was active at <12.5°. (d) The angles used to infer the geometry at which S was active (see Table 1).

[*Pérez-Gussinyé and Reston*, 2001]. Given a fault spacing of about 5 km, and fault activity over 5 Myr from the surface down to the mantle every 100 years, a dilatancy of 1 cm each time the fault is active is sufficient to pump water equivalent to 10% of the brittle volume into the mantle, enough to produce an average of 25% serpentinization of the brittle mantle. Thus, even moderate fluid influx associated with active faulting can explain the serpentinization of the mantle beneath S.

[7] The waveform inversion, depth images and modeling results show that S is a late brittle detachment of some form. The remaining questions are whether S was active during rifting and at what angle, or whether S formed by the subsequent gravitational collapse of the continental slope [*Sawyer et al.*, 2005].

3. Geometry of Movement Along S

[8] A key to understanding the origin of the S reflection is the recognition of sedimentary wedges that developed during the rotation of the crustal blocks as they moved along S. Such wedges may be synrift if developed during rifting or synsliding if S is a gravity slide, but can in either case be described as synrotational or synkinematic. The relevant synrotational wedges (orange-yellow) occur between earlier prerift or synrift units (pink) rotated with the fault block and the parallel-bedded unfaulted postrift sequence (Figures 2–4). The

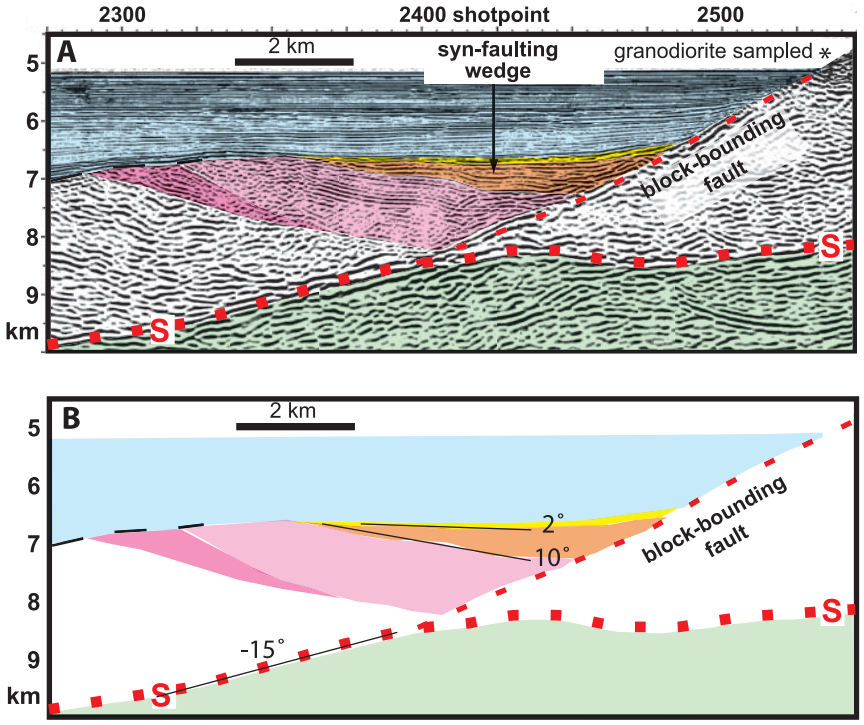

Figure 4. (a) Detail of depth migration of profile GP101 showing clear synrift wedge fanning toward a fault detaching onto S. This wedge of sediment was deposited during movement along this fault and indicates that S was active at an angle of less than 17°. Note that submersible sampling recovered granodiorite in the fault block above S. See Figure 2 for key. (b) The angles used to infer the geometry at which S was active (see Table 1).

wedges thicken toward the block-bounding faults; where clear internal fanning toward the fault is observed (orange wedges) the sediments were deposited during faulting and block rotation; for the other units it is less certain. By correcting for profile obliquity (Figure 1) and measuring dips only for the western portion of each orange wedge, we maximize the angle between S and the top of the synfaulting orange wedge to give the largest estimate of the minimum angle (15–20°) at which S was definitely active (Table 1). S was probably active at angles even lower than shown in bold. Compaction of the wedge-shaped units from c. 45% porosity (estimated from 1.8 km/s velocity of shallowest sediments) during rifting to <20% (from >3 km/s velocity of the wedges) will have increased the current eastward dip by up to 5°, implying that S was active at up to 5° lower angle than listed in Table 1. If the overlying yellow sequences (less obviously fanning) also record the geometry of the fault-detachment system, S was active at angles below 10°.

[9] Where synrift sedimentation occurs in the hanging wall of convex-upward faults detaching onto S, we expect more complicated synrift geometries associated with the fault-bend folding of the hanging wall [*Gibbs*, 1984]. Displacement along a flat-ramp (two generations of faults intersecting) and flat system (the S reflector) produces fault-bend folding of the hanging wall as it passes over the flat-ramp-flat, resulting in a hanging wall syncline depocenter above the steeper fault segment coupled with a roll-over above the S reflector [*Gibbs*, 1984; *Benedicto et al.*, 1999]. On profile ISE4 (Figure 2), just such fault-bend folding has generated an angular unconformity at the base of the synrift sedimentary sequence. The unconformity developed progressively as the Cretaceous synrift sediments onlapped the eastern limb of the syncline that developed when the hanging wall low-angle ramp was displaced by the fault above the footwall high-angle ramp (Figure 2) [*Benedicto et al.*, 1999]. This is further direct evidence that the latest steep fault detached onto a low-angle structure. Furthermore, and just as important, the reconstructions show that normal faulting occurred slowly in geological time, as it was accompanied by sedimentation, and was not a catastrophic event produced during sliding.

[10] The angle at which S developed into a detachment is constrained by the angle between S and the bases of the syntectonic wedges (Table 1; see also

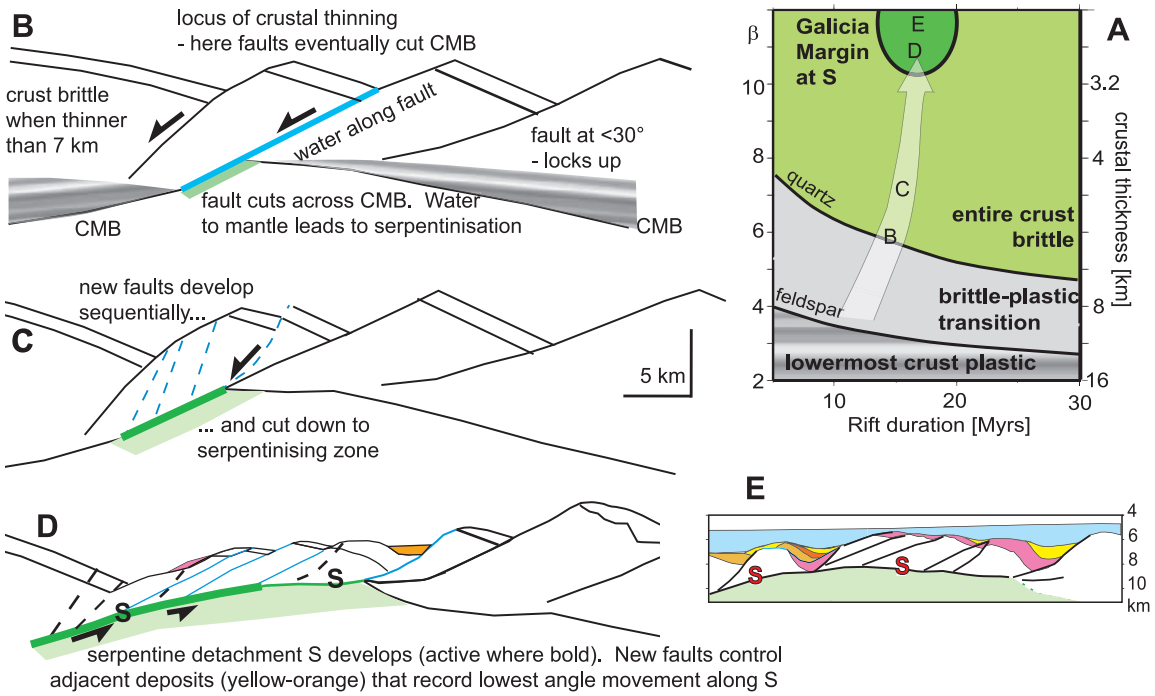

Figure 5. Schematic development of a serpentine detachment (S). (a) Embrittlement of the crust (originally 32 km thick [*Pérez-Gussinyé and Reston*, 2001]) during progressive extension (represented by arrow; labels B, C, D refer to stages shown in this figure) to form the west Galicia margin around S (dark green ellipse); plots where the entire crust has been undergoing considerable brittle extension, with faults penetrating into the mantle. (b) Possible fault block structure as crust becomes entirely brittle. Water passes along CMB-cutting fault into mantle, leading to serpentinization around the fault zone. (c) This weak serpentinizing zone acts as a detachment as new faults develop. (d) Further extension along these faults leads to generation of small fault blocks above a very gently west-dipping detachment surface (S); compare with (e) ISE4 (see also Figure 2). It is likely that the latest faults shown here developed sequentially as faulting focused toward the west.

Figures 2–4). The current geometries imply that the latest phase of extension may have started above a detachment dipping at 26 ± 15°, but allowing for internal block deformation [*Marrett and Allmendinger*, 1992] during movement along the detachment might increase this to perhaps ~30°, consistent with a reactivated weak fault zone. We thus suggest that S developed along an existing older fault (Figure 5), which is consistent with the polyphase rifting history of the margin [*Reston*, 2005]: for simple fault mechanical reasons we consider it unlikely that S formed as a new structure at this angle.

[11] The angle to which S remained active is constrained by the orientation of the synkinematic wedges (which are found in the hanging wall block of the steeper faults) relative to the orientation of S beneath the hanging wall, i.e., immediately downdip of the intersection of S with the wedge-bounding fault (Figures 2–4). Only if internal deformation and hence flattening occurred *after* fault movement (which would lead to major problems of space and structural continuity and so can be ruled out) could it have led to even a minor steepening of the angle at which S was finally active. Thus the estimates of the lowest angle at which S was active (Table 1) are probably correct: S was active at angles close to 10°.

[12] The seismic evidence all points toward the S reflector being a brittle fault that was active at low angle and which juxtaposes crustal hanging wall blocks and a serpentinite footwall. The next issue is whether S might be the basal detachment to a gravity slide (unrooted) or a rooted detachment accommodating tectonic extension.

4. Gravity Slide or Rooted Detachment

[13] *Anders et al.* [2006] argue that rapidly emplaced slides that maintain a coherent internal

Table 1. Summary of Geometry of Syntectonic (Orange) Wedges Relative to S[a]

Wedge	Character	Figure	Top Dip	Base Dip	Obliquity	App Dip S	True Dip S	Min. Dip to W S Formed	Max Dip S Still Active	Comments
ISE2	**east-fanning**	**3**	**10**	**25**	**45**	**−9**	**−12.5**	**37.5**	**<22.5**	**synfaulting**
ISE2 (yellow wedge)	overlying, poorly reflective	3	0	10	45	−9	−12.5	22.5	<12.5	if wedge synfaulting
ISE4 west	**east-fanning**	**2**	**20**	**35**	**30**	**−5**	**−6**	**41**	**<26**	**synfaulting**
ISE4 west (yellow wedge)	overlying, poorly reflective	2	~5	20	30	−5	−6	26	<11	if wedge synfaulting
ISE4 west	**east-fanning**	**2**	**20**	**35**	**30**	**−5**	**−6**	**11**	**<11**	**ramp/flat model**
ISE4 east (yellow wedge)	chaotic	2	<10	30	30	4	5	17	<5	if wedge synfaulting
GP101 SP2350	**east-fanning**	**4**	**2**	**10**	**0**	**−15**	**−15**	**25**	**<17**	**synfaulting**

[a] All measured angles are given to the east; negative numbers are dips to the west. Dips of S corrected for profile obliquity on the basis of contour map of S (Figure 1b); dips of the tops of each synrift wedge taken from the western half of the wedge, to avoid possible west-dipping depositional geometries near the fault plane itself. Differential compaction may have steepened the wedge top by up to 5°, thus causing an overestimate of the postfaulting block rotation and hence an overestimate of the angle at which S was active: S was probably active at angles even lower than calculated here from the orange synrotation sequences (bold).

stratigraphy may be mistaken for rooted detachment systems and *Sawyer et al.* [2005] raised the possibility that S might be the basal detachment to a gravity slide. In this section, we review evidence for and against a slide, concluding that S is probably not a slide, but a rooted detachment, and outlining future tests that can discriminate further.

[14] At first glance there are some reasons to suppose that S might be a slide. The block-bounding faults appear to stop at S rather than offset it, and S is a sharp reflection. Both of these observations are however also expected for a rooted detachment. The low-angle geometry is also typical of slides over evaporites or overpressured shales, but both of these are absent on this margin. The blocks above S are largely basement rather than sediment: seismic velocities within the core of the fault blocks are consistently 5–6 km/s (Figures 2a and 3a), consistent with fractured basement, and granodioritic basement has been sampled directly beneath the pretilting sediment (Figure 4). Thus a gravity slide would involve basement blocks moving at low angle over partially serpentinized peridotites exposed at the seafloor. Mechanically this might be slightly easier than movement along a rooted detachment as chrysotile is weakest ($\mu \sim 0.2$) when cool and at temperatures above 100° increases in μ to values >0.3, similar to other serpentine minerals [*Moore et al.*, 1996]. However, the thickness of the synkinematic sedimentary wedges (e.g., Figure 3c) above S and the very low sedimentation rate throughout the evolution of this margin, would imply that movement took place over many millions of years. This is not normally considered a feature of catastrophic gravity slides suggested by *Anders et al.* [2006] to be most easily mistaken for rooted detachments. Although such a duration is compatible with gravity tectonics in regions of salt or overpressured shales such as the Niger delta, salt and overpressured shales are absent here. Furthermore, during gravity sliding over millions of years, substantial thicknesses of synkinematic sediments should be affected not just by the rotational tectonics between individual blocks (forming the fanning wedges) but also the translation of those blocks, expressed as toe thrusts and folds. These are not observed.

[15] The most conclusive evidence that S is a rooted detachment would of course be to image where S roots to depth. However, this cannot be seen on the Galicia margin as S has been disrupted by later structures associated with the unroofing of the peridotites just oceanward of S (Figure 1) and subsequently by the opening of the Atlantic. Nevertheless, the probable continuation to depth of S can be identified on the conjugate SE Flemish Cap margin (Figure 6): the SCREECH 1 profile images a reflection cutting down to the NW (W in the orientation of the Galicia margin), thought from velocities to be the boundary between serpenti-

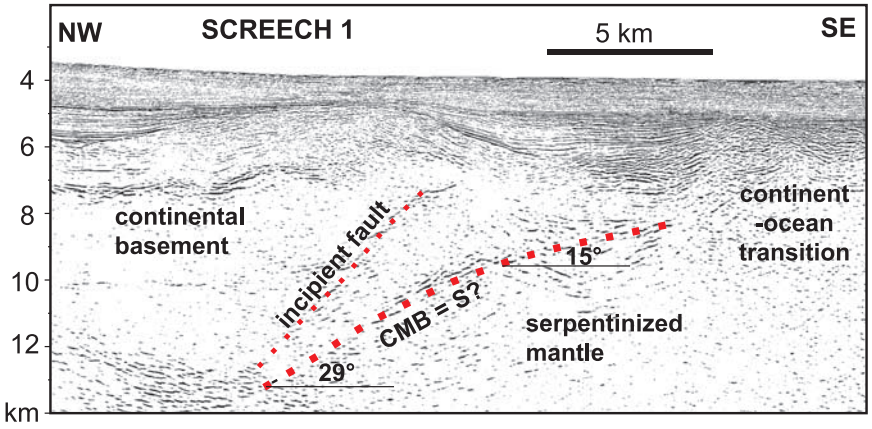

Figure 6. SCREECH 1, showing possible continuation to depth of S on the Flemish Cap margin. A NW-dipping reflection (west dipping in the orientation of the Galicia margin) corresponds to the top of serpentinized mantle (interpreted on the basis of wide-angle data) and steepens downward from 15° to just under 30°. Oceanward, the reflection is truncated by a zone of transitional crust that may be serpentinized mantle similar to the crust oceanward of S on the Galicia margin. For location, see Figure 1.

nized mantle and overlying crustal basement [*Hopper et al.*, 2004]. This structure is in a position directly analogous to a continuation of S, and dips at between 15° (near the surface) and 30° (at greater depth).

[16] Analogies with other structures support the interpretation that S is rooted. A similar structure, termed P, beneath the Porcupine Basin [*Reston et al.*, 2004] roots at 10–15° beneath the western flank of the basin: here however the lack of synrift wedges do not enable further refinement of the angle at which P was active. Wide-angle data show that the footwall to P is also probably partially serpentinized peridotites, but like S, P has never

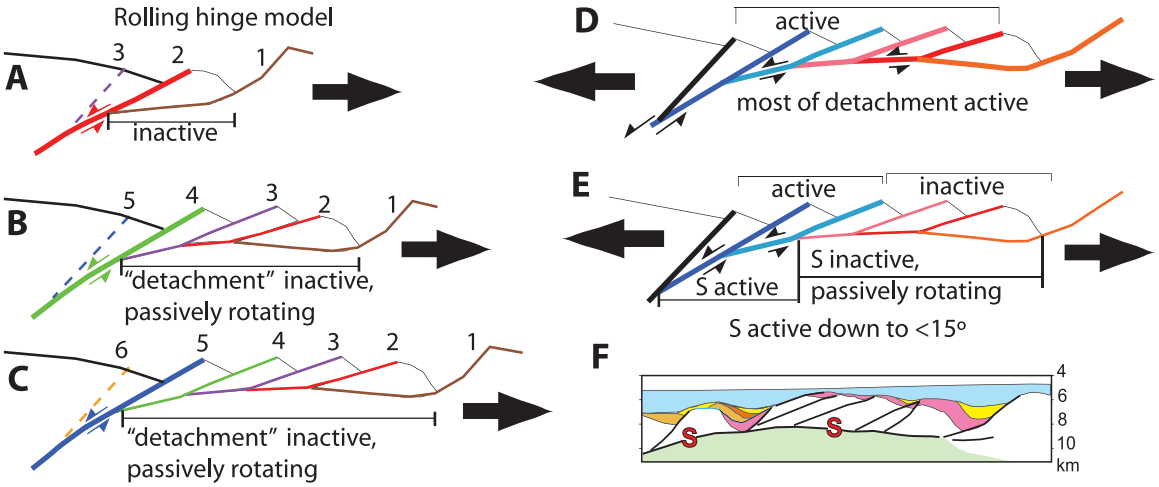

Figure 7. Rolling hinge versus standard detachment model. (a–c) Rolling hinge model for detachment fault, in which only the latest and steepest fault is active (bold). The others are passively rotating and moving as part of the footwall. Applying this model to S would still require S to be active at below 15°. (d) Classical detachment model in which all faults are active more or less simultaneously above the detachment. This model would predict that all half-grabens developed at the same time but would seem to require movement along S at unreasonably low angles. (e) Composite model in which faults gradually lock up in the east and new faults develop in the west. Several faults can be active simultaneously and detach onto an active detachment active at angles of 30° to below 15°. This model is consistent with (f) the geometry and inferred range of activity of S.

been drilled. A serpentine detachment formed at a Jurassic rifted margin, in a remarkably similar situation to S, and now exposed in the Alps, shows that the footwall to the detachment is strongly sheared parallel to the slip direction [*Manatschal et al.*, 2006]: involvement of the footwall of the detachment is expected in extensional tectonics but not in gravity sliding.

[17] In short, we cannot completely rule out the possibility that S was a gravity slide, but the available evidence suggests that it was indeed a rooted detachment fault. Further tests would include improved 3D imaging of S to determine the lateral continuity of structures above S and if possible the kinematics of movement along S (radial movement would strongly support the slide hypothesis whereas unidirectional movement would support the tectonic interpretation) through direct kinematic indicators (corrugations and striations [e.g., *Gee et al.*, 2006]), the identification of piercing points and 3D restorations. Drilling through S to assess the deformation of the footwall and the type of structure within the detachment itself [*Anders et al.*, 2006] would also constrain this issue, as would dating of the synkinematic wedges overlying S to constrain the relative and absolute timing of block movement and rotation.

5. Rolling Hinge?

[18] In the above section, we have discussed evidence that S is a rooted detachment rather than simply a gravity slide. In one end-member model, the rooted detachment was active all at one time, as the array of fault blocks moved to the west at low angle down it more or less simultaneously (Figure 7d). In another end-member interpretation (Figures 7a–7c), S might have been sequentially active as a rolling hinge [*Buck*, 1988]. In this interpretation, the footwall to S would have been flexed as it was progressively withdrawn from beneath the hanging wall, causing the fault to rotate to low angles and lock up for a new shortcut fault to propagate up from the root zone to the surface. In this manner, a succession of slices would be transferred from the hanging wall to the footwall above a detachment which became inactive as soon as the oceanward block-bounding fault developed (Figure 7), and the detachment would never have been active as a single throughgoing structure.

[19] There are a number of advantages with the rolling hinge model. First, the domal shape of S (hard to reconcile with a gravity slide) and the apparent slight postfaulting rotation of the synkinematic sediment wedges are consistent with some rotation of the system after movement locally had ceased, a prediction of the rolling hinge model. Second, the rolling hinge model is compatible with the shape of the probable root zone on the Flemish Cap margin. However the well-developed synrift wedges fanning toward the faults suggest that the faults were active over considerable time. Furthermore, if a rolling hinge model does apply, the geometries described above indicate that S was active (i.e., rooted) at low angle (<15°), and that the hanging wall splays/shortcuts must have developed while S was active at such low angles.

[20] We suspect that extension, and movement along S, was diachronous, focusing toward the west, but perhaps not as severely as in the rolling hinge model. Rather than a model in which only one fault was active at any one time, we propose that extension migrated west, causing new faults to develop there, and older faults in the east to gradually become inactive and passively rotated in the footwall to the ongoing extension. As a result, some progressive unloading of the footwall to S would have taken place, resulting in flexure to produce the slight doming observed. The different models can be distinguished most readily by dating the synkinematic wedges to determine the relative timing of movement along successive faults.

6. Angle at Which S Was Active and Fault Mechanics

[21] No matter whether S was active sequentially as in a rolling hinge model or simultaneously as in a more traditional detachment model, and indeed in both an unroofing phase and subsequently as a gravity slide, the geometries indicate that S was active at very low angle: <15°.

[22] Classical fault mechanics predict that normal faults should form at a dip of ~65°. The formation of normal faults at low angle in the absence of preexisting structures requires some modification of the regional stress field, by for instance topography or basal shear stresses, but should preclude formation of a low-angle normal fault at the same time as movement along steeper overlying structures. Furthermore, topography is not extreme, and stress refraction due to lower crustal flow and associated shear [e.g., *Westaway*, 1999] can be ruled out in an entirely brittle crust.

[23] A fault remains active as long as less stress is required for slip to occur on it than to develop a new fault. Key here are the relative friction coefficients and cohesion of the fault rocks and the unfaulted surroundings. For typical friction coefficients (0.7), a cohesionless normal fault might remain active to perhaps 35–40°. When weak minerals such as serpentine (friction coefficient as low as 0.3 [*Escartin et al.*, 2001; *Moore et al.*, 1996]) are concentrated along the fault, the fault can remain active to perhaps 17° as long as the hanging wall and footwall retain their cohesion. If they do not, and it seems unlikely that highly fractured and faulted basement will have significant cohesion after perhaps four phases of faulting and fracturing [*Reston*, 2005], the lowest serpentine slip angle is ~22° (Figure 8a). If the fractured basement also has a reduced friction coefficient, a serpentine fault will lock up at steeper dips.

[24] One way to lower the angle at which a fault remains active would be to increase the fluid pressure along the fault [*Axen*, 1992]. However, any significant increase in fluid pressure might be expected to cause hydrofracturing in the hanging wall, allowing fluids to escape and the pressure to drop [*Wills and Buck*, 1997]. We consider two different models in which fluid pressure can enable a fault to remain active at low angles.

[25] In one model, fluid pressure within and around the fault can be maintained where the hanging wall has been sealed by the growth of new minerals (especially serpentine) due to the coherent strength of those minerals [*Axen and Selverstone*, 1994]. In this model, coherent strength is effectively anisotropic, with little strength along the fault zone

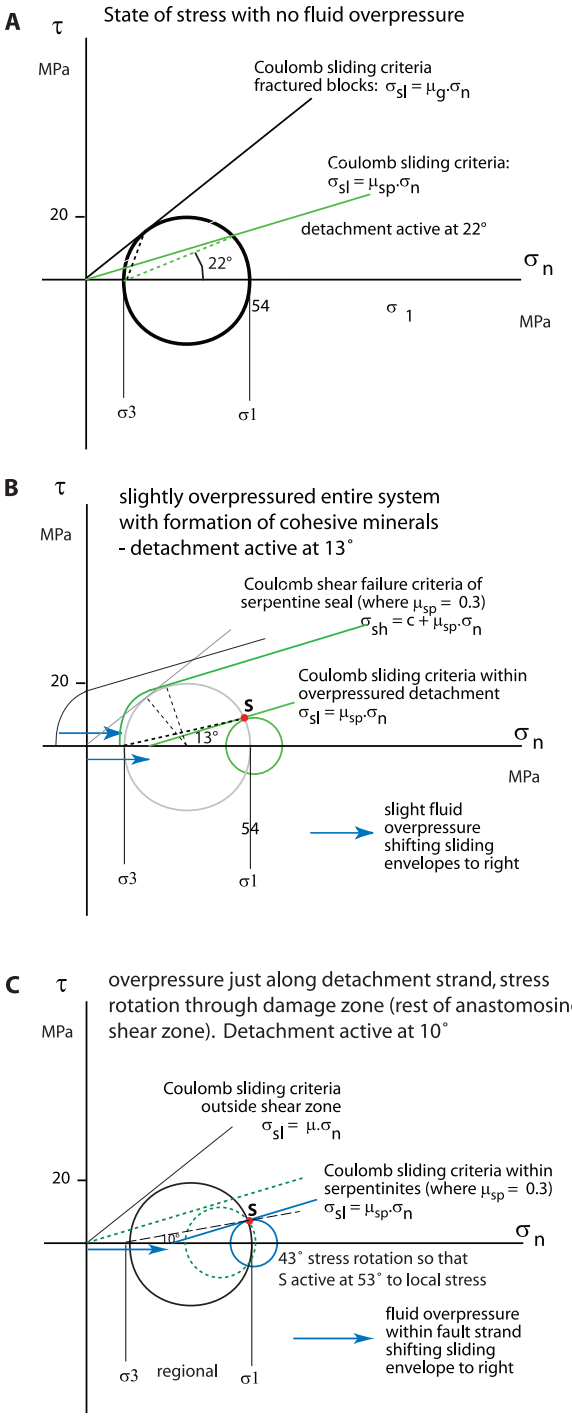

Figure 8. Mohr circle and serpentinizing fault system. (a) Mohr-Coulomb sliding criteria for fractured rock: intersection of Mohr circle (2-D stress distribution with orientation of shear zone relative to minimum principal compressive stress σ_3 (horizontal) outside shear zone) with sliding criteria (thin solid lines, slope dependent on friction coefficient) gives fault geometry (dashed lines): outside shear zone (black) and in a serpentine shear zone (green). A serpentine detachment may remain active at as low as 22° before a new fault develops. (b) Effect of development of a slight overpressure, sealed in by new unfractured mineralization, especially new serpentine minerals parallel to the shear zone (see Figure 9). These have cohesion, reduce permeability across the shear zone, and maintain moderate overpressure within the shear zone. Within the shear zone, lack of cohesion and low friction coefficient coupled with moderate fluid overpressure (blue arrows shifting sliding criteria to right) enables the detachment to move at angles as low as 13° (black dashed line) without hydrofracturing. (c) Stress rotation within damage zone (dashed green circle) approaching fault (blue circle) cause a reduction of differential stress but an increase in average stress, requiring considerable fluid pressure (blue arrows, shifting blue sliding envelope to the right) within fault to initiate fault movement at low angles.

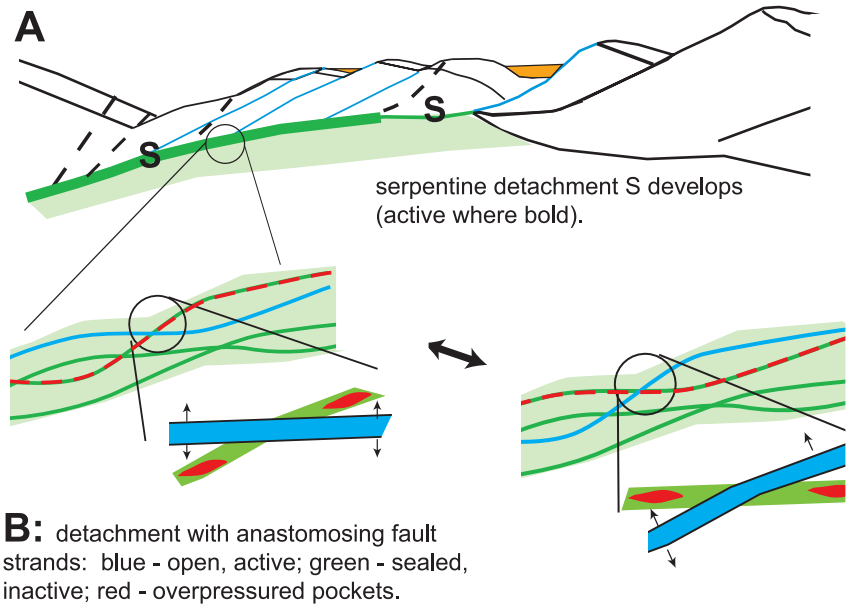

Figure 9. (a) Structure of a serpentine detachment developed beneath crustal fault blocks. (b) Detail of structure of a serpentine detachment, showing how it may consist of active (light blue) and inactive (sealed; green) strands. Volume expansion accompanying serpentinization (and resulting heating) in active strands pushes on sealed strands, leading to development of high fluid pressures in pockets (red dashes) in the latter. This leads to reopening of sealed fractures and continued movement along the anastomosing system at low angle.

(parallel to new mineral growth) and considerable coherent strength across the fault zone (across the new minerals). In this manner, an increase in fluid pressure would only lead to subvertical hydrofracturing if the cohesive strength of new minerals is exceeded. A moderate cohesive mineral strength of below 20 MPa can maintain pockets of fluid overpressure of ~15 MPa, enabling a serpentine detachment to remain active to ~13° (Figure 8b). Increasing the cohesive strength slightly and rotating the principal stress axes within the damage zone, will enable S to be active at even lower angles. Allowing the fault blocks some cohesive strength would also enable S to remain active at lower angles still.

[26] An alternative, and our preferred model, relies on stress refraction coupled with the development of fluid overpressures within the fault core (Figure 8c). Stress rotation within the fault zone would only affect stress within the detachment itself and thus not prevent hydrofracturing or other failure in the immediately adjacent rocks. However, *Faulkner et al.* [2006] show that decreasing Young's modulus and particularly increasing Poisson's ratio accompanying fracturing within the damage zone around the fault should cause stress rotation well before the fault itself is reached.

[27] In the case of anastomosing, serpentinizing detachments, the degree of both fracturing and serpentinization are likely to increase across the damage zone toward the main fault strands. Both effects are likely to lead to strong stress refraction as the Poisson's ratio of serpentine (>0.35) exceeds that of peridotite (0.25) and as Poisson's ratio increases and Young's modulus decreases as fracture density increases [*Faulkner et al.*, 2006]. A stress rotation within the "damage zone" of 40° from the regional, as documented by Faulkner et al., would enable a normal fault dipping at 10° to be active at ~50° to the local σ_1.

[28] The rotation is accompanied by an increase in the average stress toward the fault core but a decrease in the differential stress; the Mohr circle moves to the right and becomes smaller. This requires the development of locally high fluid pressure along the fault zone for this to slip, which *Faulkner et al.* [2006] relate to the low permeability of the fault core. In explaining a serpentinizing detachment, in which fluids have to penetrate the fault zone from the surface, we propose a crack-seal cycle accompanying brittle faulting (Figure 9). During and shortly after dilatant rupture, water is drawn along the fault zone from the surface, reacting with the peridotites to form serpentine. Serpentinization involves an increase in the solid

volume, is accompanied by the deposition of accessory minerals such as calcite, and is a moderately exothermic process. The last leads to an increase in the temperature of the hydrous fluids and locally increases pore pressure within the serpentinizing zone including along the detachment fault. The volume increase accompanying serpentinization and the deposition of minerals along the fault and within fractures reduce permeability, isolating segments of the fault strand and enabling local overpressure to develop within the fault, as long as the seal is not breached. Serpentinization of sidewalls accompanying movement along other open strands will increase both volume and temperature, causing pressure in the sealed strands to rise. Subsequent failure may then occur on lines of sealed fractures as a fault strand is reactivated at low angle. The pressure within the newly reopened fault strand drops as it is ruptured, but influx of further water from above will lead to further serpentinization and volume increase, jacking up the pressure along neighboring inactive fault strands until these fail and the process repeats. Just such a cycle of water influx, serpentinization, sealing, overpressure development and rupture has been inferred from sampled serpentinite fault zones [*Hopkinson et al.*, 2004]. The possibility that fluid overpressure developed along S is also supported by results from waveform inversion (Figure 3), which show that S is characterized by a LVZ underlain by a step increase in velocity. The LVZ can be interpreted as a zone of intense (~80%) serpentinization at the very top of the mantle, implying concentrated fluid flow along the S detachment and the potential for the development of transient overpressures along inactive segments of the fault.

7. Conclusions

[29] We conclude that S is a rooted detachment active at low angles, probably due to moderately elevated fluid pressures along its length. Its position, geometry and relationship to the overlying faults all indicate that S is some sort of brittle detachment. Although it cannot be demonstrated on the Galicia margin that S roots to depth, a possible continuation on the conjugate Flemish Cap margin does root downward; other evidence both here and at analogous structures elsewhere strongly suggest that S is a rooted detachment rather than a slide. Analysis of the geometry of S and of synkinematic sedimentary wedges fanning toward block-bounding faults implies that the faults detached onto S which was active at angles below 15°, too low to be explained by weak serpentinites alone. Instead it seems likely that moderately high fluid pressures may have been present along S. We suggest that slight fluid overpressure may have been maintained along the fault by the formation of new minerals, including serpentine, which act as seals. Finally, although some "detachments" may have developed as rolling hinges, the low angle at which S appears to have been active contrasts with the general form of such models. If S did develop as a rolling hinge, it was one in which the controlling fault was active at unusually low angles.

Acknowledgments

[30] This work was funded by the Deutsche Forschungsgemeinschaft under grant Re 873/6. Data collection by the R/V *Maurice Ewing* was funded by the NSF. The images presented were derived using GX Technology's SIRIUS® software. Reviews by John Hopper, Mark Anders, and Dan Lizarralde helped sharpen the arguments.

References

Abers, G. A. (2001), Evidence for seismogenic normal faults at shallow dips in continental rifts, *Geol. Soc. Spec. Publ.*, *187*, 305–318.

Anders, M. H., and N. Christie-Blick (1994), Is the Sevier Desert reflection of west-central Utah a normal fault?, *Geology*, *22*, 771–774.

Anders, M. H., N. Christie-Blick, and C. D. Walker (2006), Distinguishing between rooted and rootless detachments: A case study from the Mormon Mountains of southeastern Nevada, *J. Geol.*, *114*, 645–664.

Axen, G. J. (1992), Pore pressure, stress increase, and fault weakening in low-angle normal faulting, *J. Geophys. Res.*, *97*, 8979–8992.

Axen, G. J., and J. Selverstone (1994), Stress state and fluid-pressure level along the Whipple detachment fault, California, *Geology*, *22*, 835–838.

Benedicto, A., M. Seguret, and P. Labaume (1999), Interaction between faulting, drainage and sedimentation in extensional hangingwall-synclie basins: Example of the Oligocene Matelles basin (Gulf of Lion rifted margins, SE France), *Geol. Soc. Spec. Publ.*, *156*, 81–108.

Boillot, G., G. Feraud, M. Recq, and J. Girardeau (1989), "Undercrusting" by serpentinite beneath rifted margins: The examples of the west Galicia margin (Spain), *Nature*, *431*, 523–525.

Buck, W. R. (1988), Flexural rotation of normal faults, *Tectonics*, *7*, 959–973.

Buck, W. R., and L. L. Lavier (2001), A tale of two kinds of normal fault: The importance of strain weakening in fault development, *Geol. Soc. Spec. Publ.*, *187*, 289–303.

de Charpal, O., P. Guennoc, L. Montadert, and D. G. Roberts (1978), Rifting, crustal attenuation and subsidence in the Bay of Biscay, *Nature*, *275*, 706–711.

Escartin, J., G. Hirth, and B. Evans (2001), Strength of slightly serpentinized peridotites: Implications for the tectonics of oceanic lithosphere, *Geology*, *29*, 1023–1026.

Faulkner, D. R., T. M. Mitchell, D. M. Healy, and J. Heap (2006), Slip on "weak" faults by the rotation of regional stress in the fracture damage zone, *Nature*, *444*, 922–925, doi:10.1038/nature05353.

Floyd, J. S., J. C. Mutter, A. M. Goodliffe, and B. Taylor (2001), Evidence for fault weakness and fluid flow within an active low-angle normal fault, *Nature*, *411*, 779–783.

Forsyth, D. W. (1992), Finite extension and low-angle normal faulting, *Geology*, *20*, 27–30.

Gee, M. J. R., R. L. Gawthorpe, and S. J. Friedmann (2006), Triggering and evolution of a giant submarine landslide, offshore Angola, revealed by 3D seismic stratigraphy and geomorphology, *J. Sediment. Res.*, *76*, 9–19, doi:10.2110/jsr.2006.02.

Gibbs, A. D. (1984), Structural evolution of extensional basin margins, *J. Geol. Soc. London*, *141*, 609–620.

Hopkinson, L., J. S. Beard, and C. A. Boulter (2004), The hydrothermal plumbing of a serpentinite-hosted detachment: Evidence from the West Iberia non-volcanic rifted continental margin, *Mar. Geol.*, *204*, 301–315.

Hopper, J. R., T. Funck, and B. E. Tucholke (2004), Continental breakup and the onset of ultraslow seafloor spreading off Flemish Cap on the Newfoundland rifted margin, *Geology*, *32*, 93–96.

Krawczyk, C. M., T. J. Reston, M.-O. Beslier, and G. Boillot (1996), Evidence for detachment tectonics on the Iberia Abyssal Plain margin, in *Proceedings of the Ocean Drilling Program, Science Results*, vol. 149, edited by R. Whitmarsh, D. Sawyer, and A. Klaus, pp. 603–615, Ocean Drill. Program, College Station, Tex.

Leythaeuser, T., T. J. Reston, and T. A. Minshull (2005), Waveform inversion of the S reflector west of Spain: Fine structure of a detachment fault, *Geophys. Res. Lett.*, *32*, L22304, doi:10.1029/2005GL024026.

Manatschal, G., N. Froitzheim, M. Rubenach, and B. D. Turrin (2001), The role of detachment faulting in the formation of an ocean-continent transition: Insights from the Iberian Abyssal Plain, *Geol. Soc. Spec. Publ.*, *187*, 405–428.

Manatschal, G., A. Engström, L. Desmur, U. Schaltegger, M. Cosca, O. Muentener, and D. Bernoulli (2006), What is the tectono-metamorphic evolution of continental break-up: The example of the Tasna Ocean-Continent Transition, *J. Struct. Geol.*, *28*, 1849–1869.

Marrett, R., and R. Allmendinger (1992), Amount of extension on "small" faults: An example from the Viking graben, *Geology*, *20*, 47–50.

Moore, D. E., D. A. Lockner, R. Summers, M. Shengli, and J. D. Byerlee (1996), Strength of chrysotile-serpentinite gouge under hydrothermal conditions: Can it explain a weak San Andreas fault?, *Geology*, *24*, 1041–1044.

Mutter, J. C., C. Z. Mutter, and J. Fang (1996), Analogies to oceanic behaviour in the continental breakup of the western Woodlark Basin, *Nature*, *380*, 333–336.

Nagel, T. J., and W. R. Buck (2004), Symmetric alternative to asymmetric rifting models, *Geology*, *32*, 937–940.

Pérez-Gussinyé, M., and T. J. Reston (2001), Rheological evolution during extension at passive non-volcanic margins: Onset of serpentinization and development of detachments to continental breakup, *J. Geophys. Res.*, *106*, 3691–3975.

Reston, T. J. (2005), Polyphase faulting during the development of the west Galicia rifted margin, *Earth Planet. Sci. Lett.*, *237*, 561–576.

Reston, T. J., C. M. Krawczyk, and D. Klaeschen (1996), The S reflector west of Galicia: Evidence from prestack depth migration for detachment faulting during continental breakup, *J. Geophys. Res.*, *101*, 8075–8091.

Reston, T. J., V. Gaw, J. Pennell, D. Klaeschen, A. Stubenrauch, and I. Walker (2004), Extreme crustal thinning in the south Porcupine Basin and the nature of the Porcupine Median High: Implications for the formation of non-volcanic rifted margins, *J. Geol. Soc. London*, *161*, 783–798.

Rietbrock, A., C. Tiberi, F. Scherbaum, and H. Lyon-Caen (1996), Seismic slip on a low-angle normal fault in the Gulf of Corinth: Evidence from high-resolution cluster analysis of microearthquakes, *Geophys. Res. Lett.*, *23*, 1817–1820.

Sawyer, D. S., S. Clark, and J. K. Morgan (2005), Large scale mass wasting as a possible mechanism of formation of highly thinned continental crust and the S reflector on the Galicia rifted margin, *Eos Trans. AGU*, *86*(52), Fall Meet. Suppl., Abstract T43B-1392.

Wernicke, B. (1981), Low angle normal faults in the Basin and Range: Nappe tectonics in an extending orogen, *Nature*, *291*, 645–648.

Wernicke, B., and G. J. Axen (1988), On the role of isostasy in the evolution of low-angle normal fault systems, *Geology*, *16*, 848–851.

Westaway, R. (1999), The mechanical feasibility of low-angle normal faulting, *Tectonophysics*, *308*, 407–443.

Whitmarsh, R. B., G. Manatschal, and T. A. Minshull (2001), Evolution of magma-poor continental margins from rifting to seafloor spreading, *Nature*, *413*, 150–154.

Wills, S., and W. R. Buck (1997), Stress-field rotation and rooted detachment faults: A Coulomb failure analysis, *J. Geophys. Res.*, *102*, 20,503–20,514.

Zelt, C. A., K. Sain, J. V. Naumenko, and D. S. Sawyer (2003), Assessment of crustal velocity models using seismic refraction and reflection tomography, *Geophys. J. Int.*, *153*, 609–626.